Effect of PEGylation on the Solution Conformation of Antibody Fragments

YANLING LU,[1] STEPHEN E. HARDING,[1] ALISON TURNER,[2] BRYAN SMITH,[2] DILJEET S. ATHWAL,[2] J. GÜNTER GROSSMANN,[3] KENNETH G. DAVIS,[1] ARTHUR J. ROWE[1]

[1]National Centre for Macromolecular Hydrodynamics, University of Nottingham, Sutton Bonington LE12 5RD, England, UK

[2]UCB-Celltech, 216 Bath Road, Slough, Berkshire SL1 1NH, UK

[3]CCLRC Daresbury Laboratory, Synchrotron Radiation Department, Warrington, Cheshire WA4 4AD, England, UK

Received 16 March 2007; revised 18 May 2007; accepted 13 June 2007

Published online in Wiley InterScience (www.interscience.wiley.com). DOI 10.1002/jps.21170

ABSTRACT: Covalent attachment of poly(ethylene glycol) (PEG) to therapeutic antibody fragments has been found effective in prolonging the half-life of the protein molecule *in vivo*. In this study analytical ultracentrifugation (AUC) in combination with small angle X-ray scattering (SAXS) has been applied to a number of antibody fragments and to their respective PEGylated conjugates. Despite the large increase in molecular weight due to the attachment of a 20–40 kDa PEG moiety, the PEGylated conjugates have smaller sedimentation coefficients, s, than their parent antibody fragments, due to a significant increase in frictional ratio f/f_o (from ~1.3 to 2.3–2.8): the solution hydrodynamic properties of the conjugates are clearly dominated by the PEG moiety (f/f_o ~3.0). This observation is reinforced by SAXS data at high values of r (separation of scattering centres within a particle) that appear dominated by the PEG part of the complex. By contrast, SAXS data at low values of r suggest that there are no significant conformational changes of the protein moiety itself after PEGylation The location of the PEGylation site within the conjugate was identified, and found to be consistent with expectation from the conjugation chemistry. © 2007 Wiley-Liss, Inc. and the American Pharmacists Association J Pharm Sci 97:2062–2079, 2008

Keywords: PEGylation; immunoglobulin; antibody fragment; conformation

INTRODUCTION

Biomedical exploitation of the discrimination and affinity of antibody binding properties has been advanced by biotechnological developments. There are now 18 commercially available monoclonal antibody products and more than 100 in clinical development. In the near future, engineered antibodies are predicted to account for >30% of all revenues in the biotechnology market.[1] High-level expression systems have been developed for mammalian cell expression of antibodies; however, the large quantities needed in therapeutic doses make them prohibitively costly. Antibody fragments (Fab', Fv and scFv)[2–4] and engineered variants (diabodies, triabodies, minibodies and single-domain antibodies)[1,5–7] that can be readily produced in large-scale in microbial systems are now emerging as credible alternatives for *in vitro* immunoassays and *in vivo* tumour-targeting therapy.[8]

The improved pharmacokinetics associated with antibody fragments in tumour penetration are often modulated by the tendency of such fragments

Correspondence to: Stephen E. Harding (Telephone: +44-0-115-951-6148; Fax: +44-0-115-951-6142; E-mail: steve.harding@nottingham.ac.uk)

Journal of Pharmaceutical Sciences, Vol. 97, 2062–2079 (2008)

to have very short circulation times *in vivo*.[6] However, enhancement of the pharmaceutical properties of antibody fragments by "PEGylation", or attachment of poly(ethylene glycol) (PEG) to the fragment, appears to confer a prolonged circulating half-life on the antibody fragments.[9–13] Protein PEGylation modulates many properties of biomedical significance, including reduced toxicity, reduced immunogenicity and antigenicity; slowing rates of clearance and proteolysis, and enhancing solubility and stability (for reviews, see Refs. 14,15).

The molecular basis of the beneficial effects of PEGylation of therapeutic proteins can be attributed to the unique physicochemical properties of PEG itself (for reviews, see Refs. 16,17). One of the most distinct features of PEG is its propensity to occupy a large volume in an aqueous environment through time-averaged water association and presents a volume 5–10 times larger than a soluble protein of comparable molecular weight,[11,14,16,18,19–21] and this can confer on a protein conjugated to it advantageous features.

Numerous functionalised PEG molecules are now available commercially.[14,18,22] An appropriate choice of the size and structure of the PEG moieties and the conjugation chemistry has been found crucial to balance the desired prolonged half-life *in vivo*, while maintaining an acceptable level of relevant biological activity or activities (including not only antigen binding and antibody effector function, but also the ability to localise to certain tissues such as tumours).[10] Hence, the molecular weight of the PEG moiety, its structure, the number and location of the PEG moieties attached to the protein, as well as the chemical method of attachment, all determine the physicochemical and pharmacological properties of the resulting protein conjugate.[10,23]

Currently there are two different kinds of PEG structure—linear or branched—which can be attached to proteins. A branched structure with a single attachment site could be more favourable than the linear structure since a high molecular weight PEG moiety can apparently be obtained without increasing the number of attachment sites.[24,25] Moreover, branched chain PEGylated proteins have been found to be more stable against enzyme proteolysis than linear moieties.[23,25] Mono-site attachment of a limited number of longer chain PEG molecules rather than multisite attachment of a greater number of smaller PEG molecules has been found most beneficial for retaining a higher level of biological activity.[9,10]

Generation of PEGylated protein requires site-specific conjugation strategies to minimise the amounts of unmated isomers produced.[19,23,26] In the case of Fab' (Fig. 1) it is possible to engineer a cysteine residue in the 'residual' hinge region of the molecule (or more than one if required): to facilitate specific PEGylation through reaction between the thiol group of the cysteine and the maleimide group present in a PEG-maleimide construct to form a stable thioether linkage.[9,10,24] This reaction can generate site-specific PEGylation of the Fab' (Fig. 2) resulting in yielding a homogeneous PEGylated product preserving the full binding activities of the antibody fragment.[9]

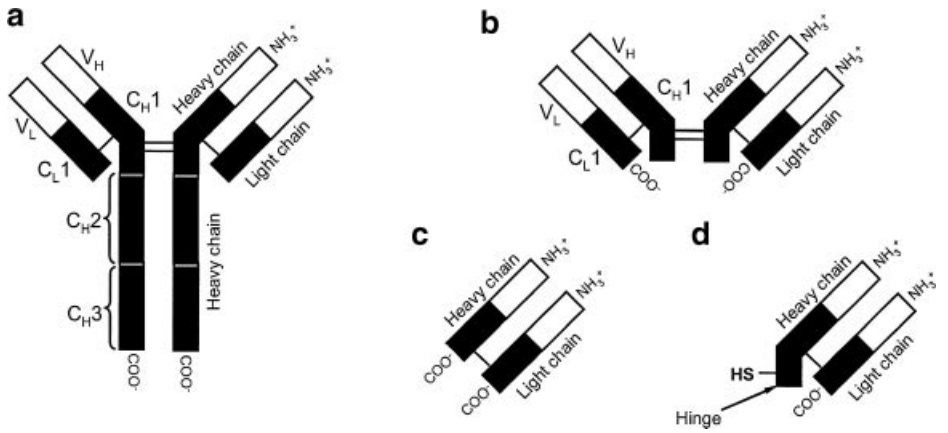

Figure 1. Schematic representation of an intact antibody molecule and some antibody fragments. (a) IgG; (b) $(Fab')_2$; (c) Fab: no hinge region, the heavy chain and light chain are linked through one disulfide bond; (d) Fab': has a short hinge region with a free cysteine.

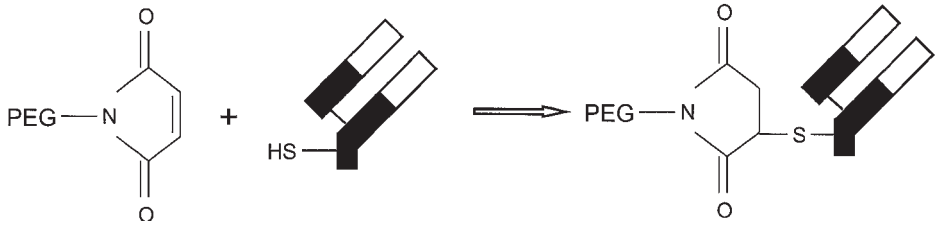

Figure 2. Schematic illustration of site-specific Fab' PEGylation. PEG-maleimide reacts with the thiol group in the hinge region of a Fab' fragment forming a stable thioether linkage.

Whilst the pharmacokinetics and pharmacodynamics of PEGylated proteins have been extensively studied, their solution properties are not as well characterised. Using thiol/maleimide conjugation chemistry a group of PEGylated antibody products has been generated to allow investigation of their solution properties and to assess if PEGylation has influenced protein conformation.

The samples were characterised using the complementary probes of analytical ultracentrifugation (AUC) and small angle X-ray scattering (SAXS). AUC can tell us about the overall hydrodynamic properties of the complexes and whether, from measurement of the sedimentation coefficient and the translational frictional ratio whether it is the protein or PEG components which dictate the properties.[27,28] This technique offers significant advantages compared to chromatographic based methods for the study of complex systems like these in that it covers a very wide range of molecular size without any requirement for known standards for calibration. There are no losses arising from macromolecule/gel matrix interactions caused by macromolecules irreversibly binding to chromatographic media, or from the failure of the conjugate molecules to be "electrophoresed" into polyacrylamide gels.

Another powerful tool we employ in this study is small angle SAXS, which probes the distribution of SAXS density in the scattering particle (see, e.g., [29,30]), allowing deductions to be made about the conformation of the scattering particles, and in particular if the effect of complexation changes the conformation of the protein component in anyway. By *combining* ultracentrifugation with SAXS, it is possible to make an assessment of the effect of PEGylation on the molecular integrity of a selection of antibody fragments.

MATERIALS AND METHODS

Production and Purification of Antibody Fragment

Three antibody fragments, human γ1 Fab'; human γ1 $F(ab')_2$ and murine γ1 Fab' and associated PEGylated products were selected for study.

Human γ1 Fab' was derived from *E. coli*: cell slurry was extracted in 0.1 M Tris/10 mM EDTA, pH 7.4 for 16 h at 30°C with constant agitation. The cells were removed by centrifugation at 10,000 rpm, for 30 min, followed by 0.22 μm filtration and adjustment to pH 7.0 using 2M Tris-HCl, pH 8.5. The Fab' was purified by application of the clarified periplasmic extract to a GammaBind G (GE-Healthcare, Chalfont St. Giles, UK) column previously equilibrated with phosphate buffered saline (PBS). The bound product was eluted with 0.1 M glycine HCl, pH 2.7, then neutralised with 2 M Tris-HCl, pH 8.5. The Fab' was quantified by absorbance at 280 nm, concentrated four-fold via ultrafiltration (UF, 10 kDa molecular weight cut-off membrane) and buffer exchanged into 20 mM Tris-HCl, pH 8.0. The diafiltered product was applied to a pre-equilibrated (20 mM Tris-HCl, pH 8.0) anion exchange column, Poros 50HQ (Applied Biosystems, Warrington, UK). The Fab' was collected in the unbound fraction, concentrated and buffer exchanged into 100 mM sodium phosphate buffer, pH 6.0 containing 2 mM EDTA, to a stock concentration of 19.5 mg/mL.

Human γ1 $F(ab')_2$ was obtained by pepsin digest of IgG and purified by gel filtration (S-200HR Amersham Pharmacia Biotech, Little Chalfont, UK). The product was concentrated and buffer exchanged into 100 mM sodium phosphate buffer, pH 6.0 containing 2 mM EDTA, to a stock concentration of 21.0 mg/mL.

Murine γ1 Fab' was mammalian derived using a NS0 cell line, grown in serum-free conditions in a

100 L fermenter. The fermenter supernatant was concentrated 10 times and then applied to a preequilibrated (20 mM sodium phosphate/150 mM sodium chloride, pH 7.1) GammaBind Plus Sepharose (GE-Healthcare) column. The Fab' was eluted with 0.1 M glycine-HCl, pH 2.8, concentrated and buffer exchanged into 100 mM sodium phosphate buffer, pH 6.0 containing 2 mM EDTA, to a stock concentration of 19.6 mg/mL.

The concentrations of the protein solutions were determined by measuring absorbance at 280 nm with extinction coefficients calculated from the amino acid compositions.

PEGylation of the Fab' fragments was achieved by site specific attachment of PEG-maleimide derivatives purchased from Nektar Therapeutics (Mountain View, CA) and NOF Corporation (Tokyo, Japan). to selectively reduced thiols. The PEGylated Fab' products used in this study are illustrated in Figure 3. *hFab'-(L)PEG25k* (Fig. 3a) was prepared by the reduction of human γ1 Fab', in 100 mM sodium phosphate buffer/2 mM EDTA, pH 6.0, using 2-mercaptoethylamine (2-MEA) at a final concentration of 5 mM for 30 min at 37°C. The reductant was removed via diafiltration (10 kDa molecular weight cut-off) into 100 mM sodium phosphate buffer/2 mM EDTA, pH 6.0. The resultant thiol was titrated using 4,4′-dithiodipyridine (DTDP) by measurement of the thiopyridine released at 324 nm; a ratio of approximately one thiol per Fab' fragment was obtained. A mono-maleimide PEG derivative with a 25 kDa linear PEG chain was added to the reduced Fab' using a molar ratio of 1.0:2.4 (Fab'/PEG) and incubated for 18 h at ambient temperature. The Fab'–PEG mixture was then adjusted to pH 4.5 by the addition of glacial acetic acid and applied to a preequilibrated (50 mM sodium acetate, pH 4.5) cation exchange column, SP Sepharose HP (Amersham Pharmacia Biotech). The product was eluted using a linear gradient of 0–250 mM sodium chloride over 20 column volumes (CV) then concentrated and buffer exchanged using a stirred cell (Amicon; 10 kDa molecular weight cut-off membrane) into 50 mM sodium chloride, 125 mM sodium chloride, pH 5.5 to a final concentration of 4.8 mg/mL, as measured by the absorbance at 280 nm. The final product was characterised by sodium dodecyl sulphate–polyacrylamide electrophoresis (SDS–PAGE) and gel filtration–high performance liquid chromatography (GF–HPLC).

hFab'-(Br)PEG2 × 20k (Fig. 3b) was prepared as described for hFab'-(L)PEG25k, except that a branched mono-maleimide PEG derivative (consisting of two linear 20 kDa chains) of overall size

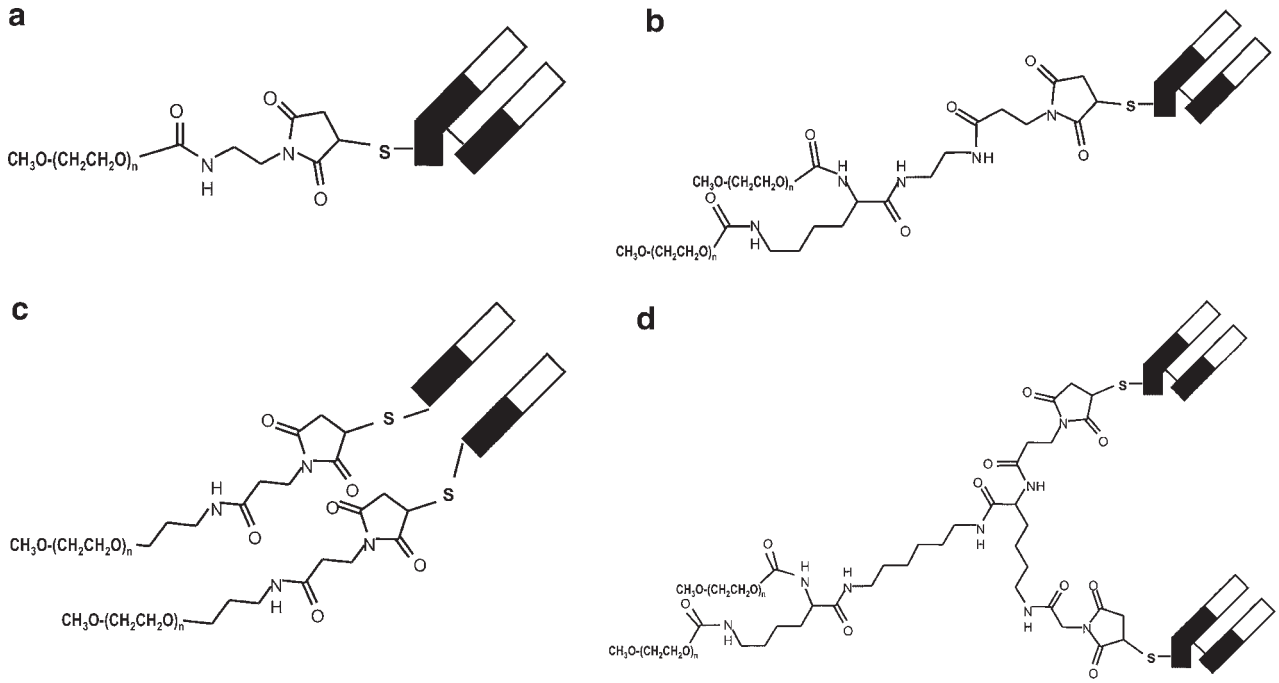

Figure 3. Schematic illustration of (a) (hFab'-(L)PEG25k); (b) (hFab'-(Br)PEG2 × 20k); (c) (mFab'-(L)PEG2 × 20k); (d) (DFM-(Br)PEG2 × 20k). CH_3–$(CH_2CH_2O)_n$– is the general structure for monomethoxy PEG (mPEG).

40 kDa was used as the PEGylation reagent. The final product was presented in 50 mM sodium acetate, 125 mM sodium chloride, pH 5.5 to a concentration of 18 mg/mL and characterised by SDS–PAGE and GF–HPLC.

mFab'-(L)PEG2 × 20k (Fig. 3c) was prepared by reduction of murine γ1 Fab' in 100 mM sodium phosphate buffer, pH 6.0 containing 2 mM EDTA using tris (hydroxypropyl)phosphine (THP,0.5 M in water, Cytec, Bradford, UK) at a final concentration of 2.5 mM for 1 h at ambient temperature. The reductant was removed via diafiltration (10 kDa molecular weight cut-off) into 100 mM sodium phosphate buffer, pH 5.7 containing 2 mM EDTA. Titration of the generated thiols with DTDP resulted in approximately two thiols per Fab' molecule due to the reduction of the interchain disulfide bond between the heavy and light chain of the Fab'. The reduced Fab' was incubated with a mono-maleimide PEG derivative with a 20 kDa linear PEG, at a molar ratio of 1.00:3.25 (Fab'/PEG) at ambient temperature for 18 h. This resulted in a product where two 20 kDa PEG chains were attached to the Fab' via the thiol at the C terminal end of the heavy chain and the light chain. Hence, there was no interchain disulphide bridge between the heavy and light chains. The Fab'–PEG mixture was then adjusted to pH 4.5 by the addition of glacial acetic acid and applied to a preequilibrated (50 mM sodium acetate, pH 4.5) SP Sepharose HP column. The product was eluted using a linear salt gradient, of 0–125 mM sodium chloride over 20 CV, concentrated and buffer exchanged into 50 mM sodium acetate, 125 mM sodium chloride, pH 5.5 to a final stock concentration of 31.7 mg/mL. The final product was characterised by SDS–PAGE and GF–HPLC.

DFM-(Br)PEG2 × 20k (Fig. 3d): The reduction was performed as described for hFab'-(L)PEG25 k. PEGylation was achieved by incubation of a bis-maleimide derivative of a branched PEG (composed of two 20 kDa linear chains) with the reduced Fab' using a molar ratio of 2.2:1.0 (Fab'/PEG) for 18 h at ambient temperature. The diFab'–PEG mixture was purified as described for hFab'-(L)PEG25 k, but using a linear salt gradient of 0–250 mM sodium chloride over 30 CV. The final product was concentrated and buffer exchanged into 50 mM sodium acetate, 125 mM sodium chloride, pH 5.5 to a final concentration of 13.5 mg/mL and was characterised by SDS–PAGE and GF–HPLC.

Concentrations of the PEGylated protein solutions were measured from measurement of ultraviolet (UV) absorbance at a wavelength of 280 nm. The extinction coefficient of the PEG is negligible as pure PEG revealed a minimal signal contribution,[11] therefore a weight-averaged extinction coefficient was used for each PEGylated molecule by taking into account the contribution of the mass of the PEG to the conjugate. For instance, in the case of mFab-(L)PEG2 × 20k, at 280 nm the extinction coefficient of the Fab' alone is 1614 $mL\,g^{-1}\,cm^{-1}$, and taking into account the mass contribution of the 40 kDa PEG, the weight-averaged extinction coefficient for mFab-(L)PEG2 × 20k is 873 $mL\,g^{-1}\,cm^{-1}$.

The commercial manufacturers claim for the molecular weight of the branched PEG (2 × 20 k) of 40 kDa was checked by both size exclusion chromatography coupled to multi-angle laser light scattering (courtesy of Dr. G. Morris, NCMH) yielding a value for the weight average molecular weight M_w of (40.5 ± 1.2) kDa.

Table 1 lists the PEGylated conjugates used in this study. The partial specific volume $\bar{\nu}$ of each antibody molecule was calculated using the routine SEDNTERP[31] from the amino acid composition. Following Lepori and Mollica[32] and Nichol et al.,[33] a value of 0.83 mL/g was used as the partial specific volume for the all the PEG molecules evaluated. The weight-averaged partial special volume for each of the PEGylated

Table 1. Molecular Weights *M* and Partial Specific Volumes $\bar{\nu}$ of PEGylated Antibody Fragments

Sample	Attached PEG (kDa)	Molecular Weight *M* (kDa)	$\bar{\nu}$ (mL/g)
Murine γ1 Fab'	0	47	0.726
Human γ1 Fab'	0	48	0.726
Human γ1 $F(ab')_2$	0	96	0.726
mFab-(L)PEG2 × 20k	40	87	0.774
hFab'-(L)PEG25 k	25	73	0.762
hFab'-(Br)PEG2 × 20k	40	88	0.777
DFM-(Br)PEG2 × 20k	40	136	0.759

conjugates (see Table 1) was then calculated using the following relation:[34]

$$\overline{\nu}_c = \sum_{i=1}^{N} f_i \overline{\nu}_i = f_p \overline{\nu}_p + f_{np} \overline{\nu}_{np} \quad (1)$$

where f_p and f_{np} are the weight fractions of protein and nonprotein components respectively, and $\overline{\nu}_p$ and $\overline{\nu}_{np}$ their partial specific volumes.

SDS–PAGE and HPLC Analysis of PEGylated Antibody Fragments

The Fab' fragments and their associated PEGylated products were analysed for purity by SDS–PAGE and GF–HPLC prior to the hydrodynamic studies.

SDS–PAGE was performed using Novex Tris-Glycine (4–20%) gels (Invitrogen EC60255BOX, Paisley, UK) under both nonreducing and reducing conditions. For nonreducing conditions 10 μL of a 0.4 mg/mL solution of the sample was diluted 1:1 with Tris-Glycine SDS Sample buffer x2 (Invitrogen LC2676) and boiled for 2 min; for reducing conditions 2.2 μL of NuPage Sample Reducing Agent × 10 (Invitrogen NP0004) was included in the nonreducing mixture and boiled for 3 min. In both cases 10 μg was loaded onto the gel and ran according to the manufacturer's instructions (a constant voltage of 125 V for 90 min). The bands on the gel were visualised by Coomassie Blue staining.

GF–HPLC was performed using an HPLC system (Agilent 1100, Stockport, UK) with Zorbax GF450 (Agilent 884973-902) and Zorbax GF250 (Agilent 884973-901) columns connected in series. The elution buffer was 0.2M sodium phosphate, pH 7.0 containing 10% ethanol. The samples were analysed at 1.0 mL min^{-1} isocratically with a 30 min run time, at a wavelength of 280 nm.

Sedimentation Velocity and Equilibrium in the Analytical Ultracentrifuge

All Fab' fragments and their associated PEGylated products were diluted to between 0.5 and 1.6 mg/mL at six different concentrations prior to sedimentation velocity experiments in an Optima XLA (Beckman Instrument, Palo Alto, CA), at 20°C using an An60Ti four-place rotor running at various rotor speed (45000 rpm for velocity runs and 12000–14000 rpm for equilibrium runs). The sedimentation process was monitored by UV absorbance with a scan interval of 4 min, with the buffer as the reference solvent. Absorption optics was chosen for studying PEGylated antibodies as PEG had minimal signal contribution at 280 nm[11]: any unconjugated PEG would not be detected.

We also investigated the sedimentation coefficient behaviour of the linear "20 kDa" (molecular weight estimated by the manufacturer) PEG reagent (see Fig. 3b) and the branched "40 kDa" PEG reagent (see Fig. 3c) using the interference optical system on an Optima XLI (Beckman Instrument). The 20 and 40 kDa PEG samples (in powder form) were dissolved separately in 50 mM sodium acetate, 125 mM sodium chloride buffer (pH5.5) and concentrations were determined using an Atago DD-5 differential refractometer (Jencons Scientific, Leighton Buzzard, UK) (dn/dc = 0.134 mL/g). Samples were then diluted to between 0.3 and 2.3 mg/mL prior to the velocity run at 50000 rpm.

Sedimentation velocity data were analysed by the so-called least squares $g^*(s)$ or "ls-$g^*(s)$" procedure as implemented in SEDFIT.[35,36] $g^*(s)$ profiles confirmed the monodispersity and the aggregate-free nature of the solutions (see Discussions later), which are critical for the subsequent interpretation of the SAXS data. The experimental sedimentation coefficient values $s_{20,b}$ (the designation $s_{20,b}$ to indicate that the value reported applies to conditions of 20.0°C in a solvent b, which in this case is the formulation buffer) obtained from SEDFIT have been corrected to $s_{20,w}$ (standard solvent conditions—the density and viscosity of pure water at 20.0°C) using SEDNTERP.[31] The $s_{20,w}$ values obtained at different concentrations were extrapolated to zero concentration to yield $s^0_{20,w}$ thereby eliminating solution nonideality effects.[37]

Sedimentation equilibrium data were evaluated by the model-independent routine MSTARA[38]—no model (ideal, single solute, etc.) has to be assumed *a priori*, as required by other software. Determination of the baseline absorption by over-speeding the centrifuge was necessary to correct for UV-absorbance from nonmacromolecular material. At each loading concentration, the MSTARA program provides a plot of $M^*(r)$ versus $\xi(r)$ for determination of molecular weight, where $M^*(r)$ is an operational point average molecular weight and $\xi(r)$ is the radial displacement squared parameter defined by:

$$\xi(r) = \frac{(r^2 - r_a^2)}{r_b^2 - r_a^2} \quad (2)$$

where r_a, r_b are the radial positions of the cell meniscus and cell base, respectively. Although the $M^*(r)$ values themselves have no physical meaning, the $M^*(r)$ extrapolated to the cell base ($\xi(r) = 1$) yields the apparent weight-average molecular weight over all the macromolecular components in the ultracentrifuge cell, M_w.[39] M_w at different concentrations were extrapolated to zero concentration to eliminate any contribution from thermodynamic nonideality.[37]

Small Angle X-Ray Scattering (SAXS)

The SAXS data were obtained at Station 2.1 at the Synchrotron Radiation Source (SRS, Daresbury, UK), employing sample-to-detector distances of 1 m (to cover a scattering range of $0.04 < Q < 0.30$ Å^{-1}) and 4 m (for $0.009 < Q < 0.19$ Å^{-1}). Q is the magnitude of the scattering wave vector and defined as $Q = 4\pi \sin \Theta/\lambda$, where 2Θ is the total scattering angle relative to the forward direction and λ the X-ray wavelength. The detector was calibrated with wet rat-tail collagen (characteristic spacing of 670 Å) and silver behenate (characteristic spacing of 58.38 Å). Data were collected at different antibody concentrations on the 1 m camera in 60 s time frames (ranging from 4.8 to 31.7 mg/mL) and on the 4.0 m camera in 20–10 s frames (ranging from 1.29 to 9.5 mg/mL). Using the standard Daresbury software package XOTOKO,[40] the data were then normalised to the intensity of the incident beam, radially averaged, and corrected for the detector response. The total scattering intensity from each of the time frames was determined to check for beam induced aggregation in the sample, those frames showing increasing counts were excluded from further analysis as the increase was considered to be due to radiation induced aggregation.

After subtracting the buffer contribution to correct for the inter-particle interaction effects in the low-angle region of the high concentration measurement, the low-angle regions of the low concentration data were scaled to merge with the high-angle region of the high concentration data using SigmaPlot® (Systat Software, Inc., San Jose, CA). The distance distribution function p(r) and the maximum dimension (D_{max}) of the scattering particle were obtained by using GNOM.[41] The radii of gyration (R_g) were determined by using the Guinier approximation with data from the low angle region,[42] and from transformation of the entire scattering profile with GNOM.

It suffers the disadvantage over AUC in that larger amounts of material are required. For this reason, although we were able to study all the samples by AUC, SAXS studies were possible on five out of the seven preparations.

Ab Initio Modelling

Ab initio shape reconstruction (i.e. without prior knowledge of shape) from the angular scattered intensity envelope has proved useful in representing the solution conformation of complex macromolecules of different topologies.[30] Among the various *ab initio* reconstruction algorithms existing, the program DAMMIN[43] was used in our study. DAMMIN calculates the scattering intensities of a particle built up from a finite number of dummy beads and minimises the surface between the particle and the solvent. Ten low resolution models obtained from different DAMMIN runs were analysed following procedures described in Ref. 44 and the stable constructions were averaged using the program DAMAVER[44] which yields an average model representing the common characteristic structural features of all the reconstructions.

The atomic coordinates of the crystallographic models of two Fab' molecules were taken from the Brookhaven Protein Data Bank (accession code 1UCB and 1BBJ respectively) and the scattering profiles of these two models were calculated using CRYSOL[45] and HYDROPRO.[46] The *ab initio* model for the murine γ1 Fab' was then superimposed onto these crystallographic models using the programs SUPCOMB[47] and MASSHA[48] to check the validity of the *ab initio* shape reconstruction. For the PEGylated Fab' or Fab' molecule, the averaged shape model was superimposed onto the model of murine γ1 Fab' after alignment using SUPCOMB. In the case of *DFM-(Br)PEG2 × 20k*, as no scattering data was available on DFM, comparison was made by superimposing the model of the human γ1 F(ab')$_2$ onto the DFM-(Br)PEG2 × 20k.

RESULTS

SDS–PAGE and GF–HPLC Analysis of PEGylated Antibody Fragments

SDS–PAGE analysis of human γ1 Fab' and associated PEGylated species can be seen in Figure 4. The human γ1 Fab' preparation shown

 DOI 10.1002/jps

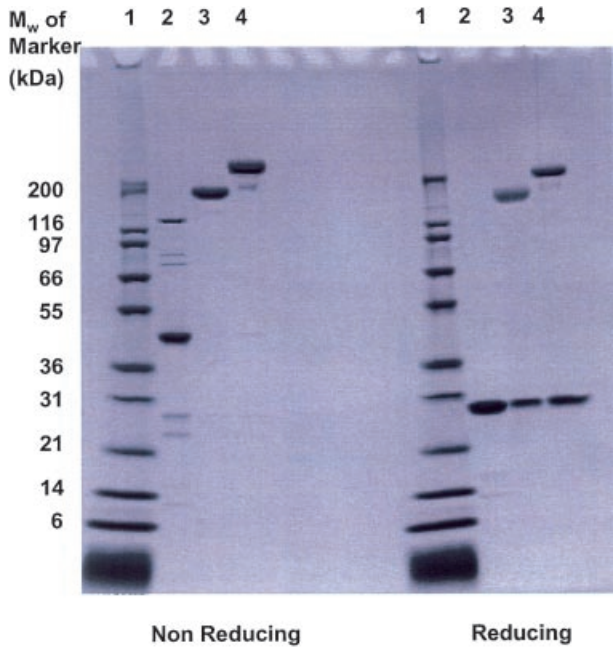

Figure 4. SDS–PAGE analysis (NOVEX™, Tris/Glycine 4–20%) of human γ1 Fab' and associated PEGylated conjugates under nonreducing and reducing conditions. Lane 1, molecular weight marker (Mark12™, NOVEX™); (Lane 2) human γ1 Fab'; (Lane 3) hFab'-(Br)PEG2 × 20k; (Lane 4) DFM-(Br)PEG2 × 20k. Left panel, nonreducing conditions; (right panel) reducing condition.

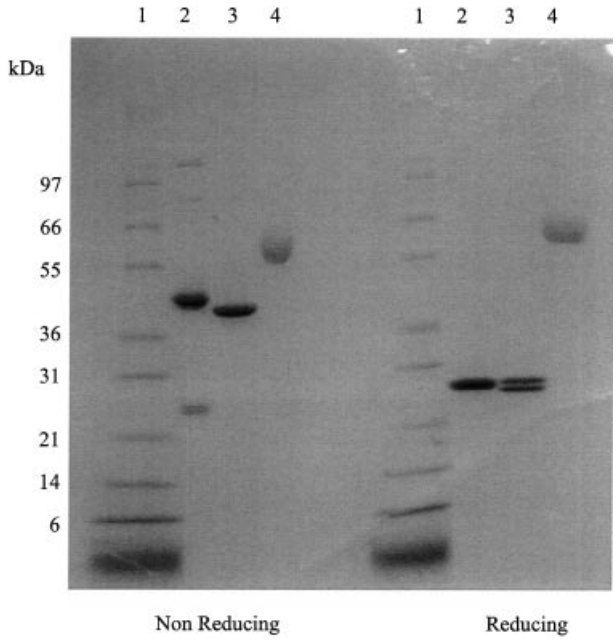

Figure 5. SDS–PAGE (Tris-Glycine 4–20%) analysis of murine γ1 Fab' and its associated PEG conjugates under nonreducing and reducing conditions. Lane 1, molecular weight markers (Mark 12); (Lane 2) human γ1 Fab'; (Lane 3) murine γ1 Fab'; (Lane 4) mFab'-(L)PEG2 × 20k

in Lane 2 was seen to contain some $F(ab')_2$ evidenced by a band at approximately 100 kDa: there was also evidence for some free heavy and light chains at approximately 25 kDa. The associated PEGylated components in Lanes 3 and 4 are shown to be >95% pure. The contamination of the human γ1 Fab' has no consequences in terms of interpretation of sedimentation coefficients as the other components resolve away but renders opaque to interpretation the SAXS records. By contrast, both the murine γ1 Fab' and mFab'-(L)PEG2 × 20k were >99% pure (Fig. 5). The mobility of the mFab'-(L)PEG2 × 20k (Lane 4) was equivalent in both nonreducing and reducing conditions confirming that there was no disulphide bridge between the heavy and light chains and that a 20 kDa linear PEG chain was attached to the C terminal end of both the heavy and light chain.

The results of GF–HPLC analysis for both human γ1 Fab' and murine γ1 Fab' with associated PEGylated products can be seen in Figures 6 and 7. GF–HPLC analysis of human γ1 Fab' (Fig. 6), confirmed the presence of $F(ab')_2$ (28%). The PEGylated species, hFab'-(Br)PEG2 × 20k, DFM-(Br)PEG2 × 20k and hFab'-(L)PEG25 k (not shown) were shown to be>98% pure. For the murine γ1 Fab' and mFab'-(L)PEG2 × 20k (Fig. 7), both species were shown to be >99% pure.

Hydrodynamic Behaviour of PEGs

Figure 8 shows an example of the $g^*(s)$ distribution for the branched 40 kDa PEG plotted with respect to s (Fig. 8a) and $\log_e s^2$ (Fig. 8b), where the latter takes into account we are dealing with a quasi-continuous log-normal distribution of molecular weights for the PEG.

The conformation of the PEG chain in aqueous solution is still a matter of debate. X-ray structural analysis has shown that crystalline PEG chains can adopt two extreme structural conformations: a zigzag, random coil structure for shorter chains, or a winding, helical structure for longer chains.[49] It has been argued from earlier studies that viscosity[50–53] and diffusion coefficient data[50] support a random coil conformation,

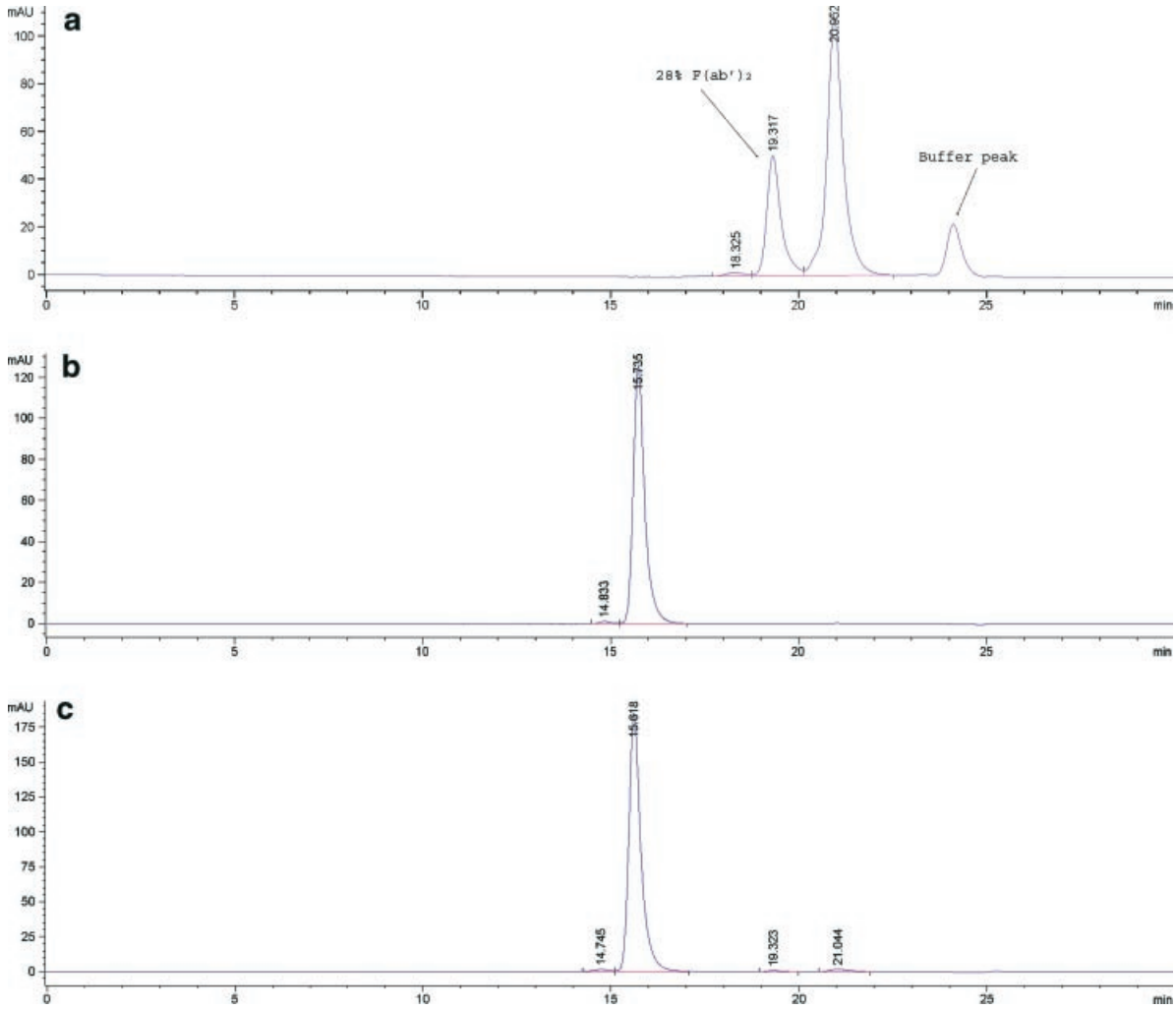

Figure 6. GF–HPLC analysis of (a) human γ1 Fab'; (b) hFab'-(Br)PEG2 × 20k; (c) DFM-(Br)PEG2 × 20k. Zorbax GF450/GF250 HPLC columns in series with isocratic elution in 0.2 M sodium phosphate, pH 7.0/10% ethanol at 1.0 mL min^{-1}, detected at a wavelength of 280 nm.

whereas it has been claimed from calorimetric data[54] that it adopts a helical conformation. Based on volumetric studies, Lepori and Mollica[32] favour a compromise model for PEG in solution is a hydrated flexible coiled polymer with some helical segments.

In many cases with high polymeric solutes there is a unique relation between the sedimentation coefficient s and the molecular weight M. For example the extremes are as follows (see, e.g. Ref. 55):

$$\text{Compact sphere} : s \sim M^{0.667} \tag{3}$$

$$\text{Rigid rod} : s \sim M^{0.15} \tag{4}$$

For a flexible coil polymer, s and M follows the relation that[55]

$$s \sim M^{0.4-0.5} \tag{5}$$

or to an approximation

$$s^2 \sim M \tag{6}$$

In all three cases $\log_e(s)$ is the appropriate abscissa. Therefore if the PEG moiety investigated in this study is approximately a random coil conformation, and contains a continuous log-normal distribution of polymer chain lengths,[56] we would expect the $g^*(s)$ distribution plot on a $\log(s^2)$ scale (or 2 $\log(s)$) which in turn mirrors the

 DOI 10.1002/jps

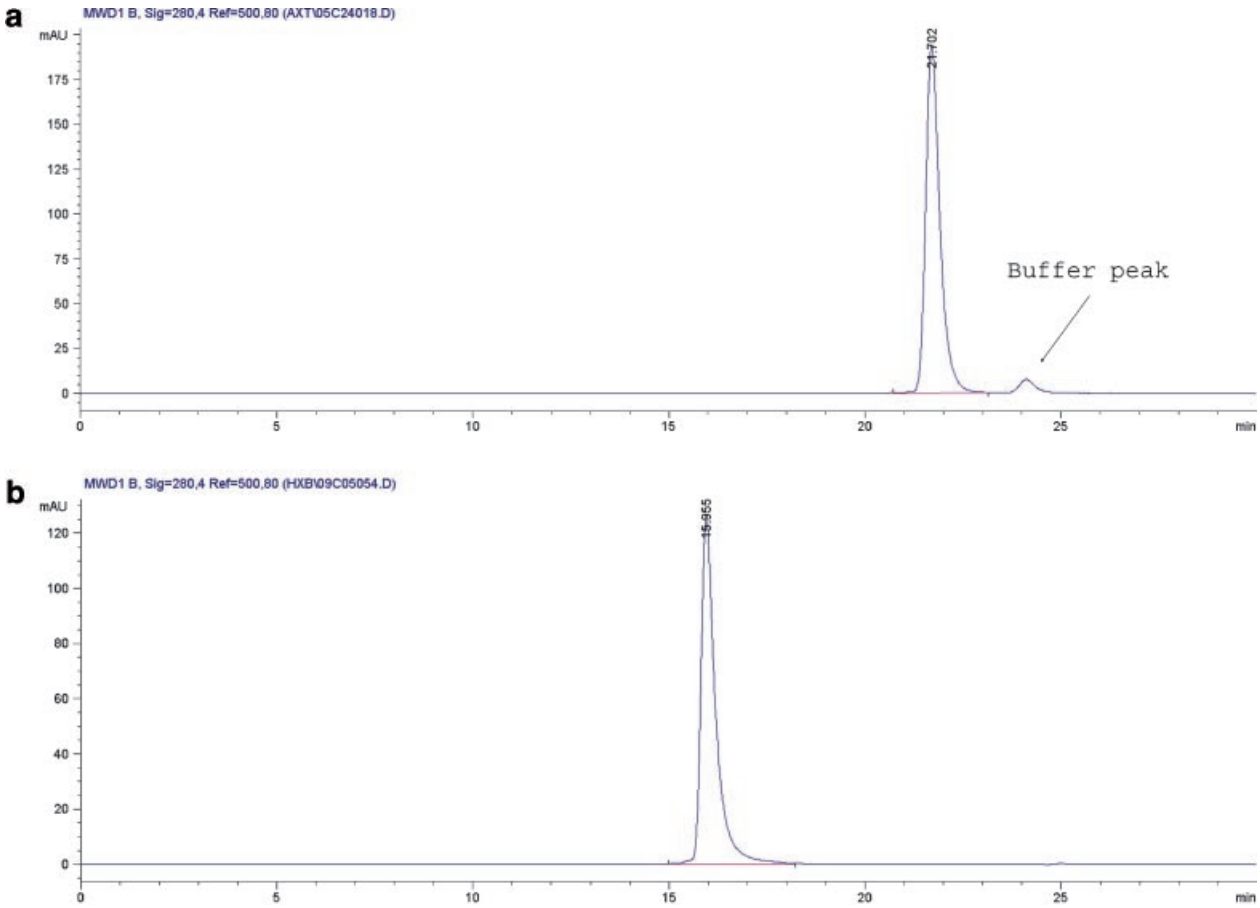

Figure 7. GF–HPLC analysis of (a) murine γ1 Fab' and (b) mFab'-(L)PEG2 × 20k. Zorbax GF450/GF250 HPLC columns in series; isocratic elution in 0.2 M sodium phosphate, pH 7.0/10% ethanol at 1.0 mL min^{-1}; detected at a wavelength of 280 nm.

normalised molecular weight distribution to be a unimodal Gaussian distribution. This unimodal Gaussian distribution feature (see, e.g. Fig. 8b) is clearly evident within the range of concentrations studied (from 0.6 to 2.3 mg/mL). The slight deviation could due to the diffusive effects.

The $g^*(s)$ distribution yields a modal sedimentation coefficient. For both PEG reagents, considerable nonideality effects were observed as the sedimentation coefficient showed a marked decrease with increasing concentrations (data not shown). The concentration-dependence coefficient k_s estimated from the extrapolation of 1/*s* versus *conc*. plot to zero concentration yields a value of (81 ± 6) mL/g using the relation

$$\frac{1}{s} = \frac{1}{s^0} + \frac{k_s}{s^0} c \tag{7}$$

This high k_s value found for the 40 kDa PEG is much larger than for globular proteins which confirms the flexible expanded conformation of the molecule. Extrapolations of the 1/*s* versus *conc*. plot to zero concentration yields an $s^0_{20,w}$ value of (0.64 ± 0.01)S for the linear 20 kDa PEG reagent and (0.82 ± 0.01)S for the branched 40 kDa PEG reagent. Interestingly, it is possible to estimate the molecular weight M based on the $s^0_{20,w}$ and k_s (after correction for radial dilution) measurements:[37] for the 40 kDa PEG reagent, a value of $M \sim$39000 g/mol is returned.

The sedimentation coefficient is inversely proportional to the frictional ratio following the relation:

$$s^0_{20,w} = \frac{M_w(1 - \bar{\nu}\rho_0)}{6\pi N_A \eta_0} \left(\frac{4\pi N_A}{3\bar{\nu}M_w}\right)^{1/3} \frac{1}{f/f_0} \tag{8}$$

where M_w is the weight averaged molecular weight (g/mol), $\bar{\nu}$ is the partial specific volume (mL/g), N_A is Avogadro's number (6.02205×10^{23} mol^{-1}), ρ_0 (g/mL) and η_0 (Poise) are the density and viscosity of water at 20.0°C respectively.

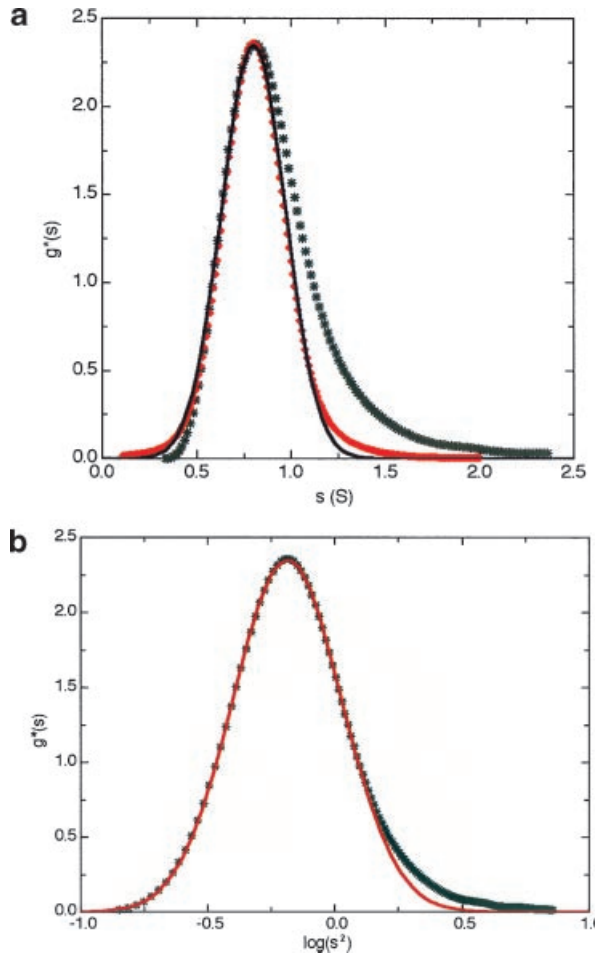

Figure 8. ls-$g^*(s)$ distribution of a 0.57 mg/mL 40 kDa PEG solution. (a) plotted versus s; (b) plotted versus $\log(s^2)$, Green: experimental $g^*(s)$ distribution; red: simulated data from SEDFIT[35,36] and black solid lines shows a single Gaussian curve. Simulated data generated from SEDFIT is based on a single-component system (using $M_w = 40$ kDa and $s = 0.8$S), showing the broadening of the peak is due to diffusion alone.

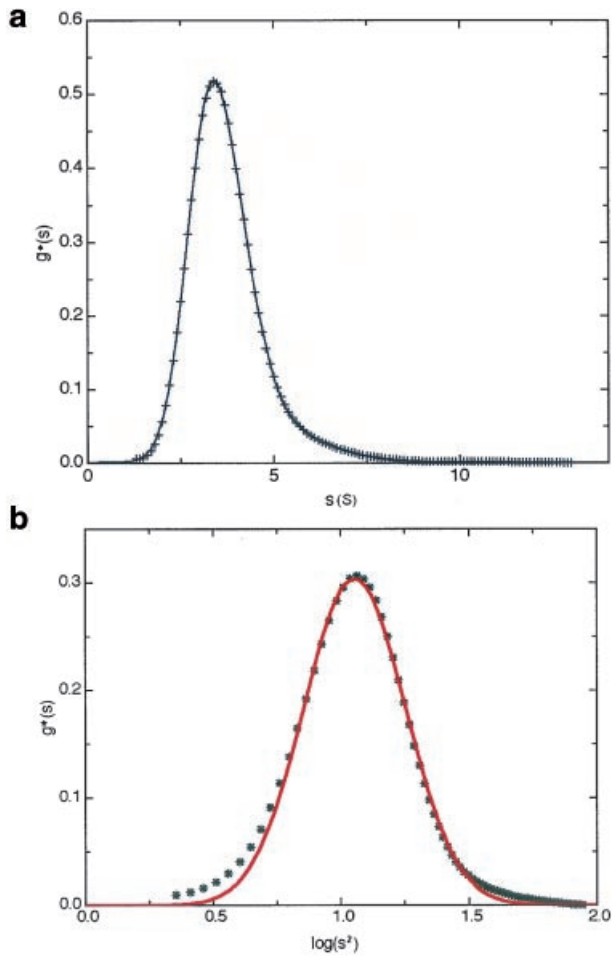

Figure 9. The ls-$g^*(s)$ distribution for a 1.2 mg/mL *hFab'-(Br)PEG2 × 20k* solution. (a): $g^*(s)$ versus s distribution. (b): log-normal distribution. In (b) the * line is the experimental distribution and the red solid line shows a single Gaussian curve.

Following this relation, high frictional ratios (ratio of the actual friction experienced by a particle moving through a fluid to the friction which it would experience if it were a compact sphere of the same mass)[57] were found for the 20 kDa PEG ($f/f_o \sim 2.5$) and the 40 kDa PEG ($f/f_o \sim 3.0$) using the algorithm UNIVERSAL_PARAMS.[58]

Hydrodynamic Behaviour of PEGylated Conjugates

Interestingly, sedimentation velocity analyses of the PEGylated antibody solutions reveal their homogeneous nature. Moreover, the $g^*(s)$ distribution of these PEGylated antibodies mirrors the effect seen in the analysis of PEG that the distribution is log-normal with respect to s or s^2 (an example see Fig. 9). This suggests that the hydrodynamic behaviour of PEGylated antibody is predominantly dictated by the attached PEG moiety. Again, similar to the 40 kDa PEG, the modal sedimentation coefficients obtained from $g^*(s)$ distribution at different concentrations were extrapolated to zero concentration to eliminate the effect of nonideality, and the $s^0_{20,w}$ values are reported in Table 2.

The weight-average molecular weights of the PEGylated conjugates from sedimentation equilibrium are also shown in Table 3. Despite

Table 2. Experimental Sedimentation and X-Ray Scattering Data for the Antibody Fragments and their PEGylated Conjugates

Sample	$s^0_{20,w}$ (S)	f/f_o	R_g (Å)	D_{max} (Å)
Murine γ1 Fab'	3.67 ± 0.02	1.30	26.4 ± 1.0	76 ± 2
Human γ1 Fab'	3.95 ± 0.01	1.23	—	—
Human γ1 F(ab')$_2$	5.49 ± 0.01	1.40	41.0 ± 1.0	117 ± 3
mFab-(L)PEG2 × 20k	2.12 ± 0.02	2.75	29.5 ± 1.0	94 ± 2
hFab'-(L)PEG25 k	2.40 ± 0.01	2.29	31.2 ± 1.0	96 ± 2
hFab'-(Br)PEG2 × 20k	2.16 ± 0.02	2.68	—	—
DFM-(Br)PEG2 × 20k	3.41 ± 0.03	2.47	49.6 ± 1.0	145 ± 3

$s^0_{20,w}$: sedimentation coefficient; R_g: radius of gyration, D_{max}: maximum dimension of the scattering particle.

the polydisperse nature of the PEG reactants, the measured molecular weight and the theoretical values for the PEGylated molecule are in reasonable agreement.

Solution Conformation of Antibody Fragments and PEGylated Conjugates

Sedimentation Coefficients

The sedimentation coefficient ($s^0_{20,w}$) is a manifestation of the overall size and shape of a macromolecule in solution and the data from our experiments are summarised in Table 2. The value for human γ1 Fab' (3.95 ± 0.01)S is similar to previous determinations.[59] With its short hinge removed, murine γ1 Fab' sediments at the same rate (3.67 ± 0.02)S as murine classic γ2a Fab' (3.68 ± 0.01)S.[60] Comparison of these last two values indicate that the existence of the hinge may not alter the overall conformation of the antibody fragment and the difference in the hydrodynamic behaviour between human γ1 Fab' and murine γ1 Fab' is ascribed to the different antibody species used. It is worth pointing out that the murine γ1 Fab' has no upper or middle hinge region since a stop codon was inserted in the gene after the CYS residue in CH1. Interestingly, human γ1 F(ab')$_2$ has an identical sedimentation coefficient (within experimental error) to the DFM (covalently linked diFab'-maleimide) of (5.53 ± 0.04)S (Harding, S.E. and Rhind, S.K. unpublished work).

Despite a large increase in molecular weight due to the conjugation of either linear 25 kDa or branched 40 kDa PEG moieties with the proteins, both *hFab'-(L)PEG25k* and *hFab'-(Br)PEG2 × 20k* sediment at a slower rate compared to the parent antibody human γ1 Fab' (see Table 2). Similar sedimentation behaviour has been observed for the *mFab'-(L)PEG2 × 20k* and *DFM-(Br)PEG2 × 20k*. These data suggest a significant effect of PEG on the conformation of all the antibody fragments studied, with the increase in frictional ratio f/f_o (from ~1.3 to 2.3–2.8): the solution hydrodynamic properties of the conjugates are clearly dominated by the PEG moiety (f/f_o ~3.0).

Unfortunately quantifying further the effect on conformation is rendered difficult because of the effects of addition of the PEG on the water association or time averaged "hydration" of the antibodies—which also increases the frictional ratio. The large hydrodynamic size or volume of PEGylated antibodies in solution has already been reported.[10]

Table 3. Molecular Weights of the PEGylated Conjugates

Sample	Theoretical M (Da)	M_w (Da)
mFab-(L)PEG2 × 20k	87200	78000 ± 3000
hFab'-(Br)PEG2 × 20k	88100	82000 ± 4000
hFab'-(L)PEG25 k	73100	73000 ± 2000
DFM-(Br)PEG2 × 20k	136100	125000 ± 4000

M_w: experimental (weight-average) molecular weight from sedimentation equilibrium.

Small Angle X-Ray Scattering

Although the complexities of hydration and flexibility render it difficult to comment on the detailed conformation of the protein-PEG conjugates it is nonetheless possible to provide limited but nonetheless useful information on the conformation of the protein moiety and the location of the PEGylation site within the complex, using SAXS to extend the sedimentation velocity data.

Small angle SAXS measures the relative scattering intensity between the scattering particle and the solvent.[29] The Guinier approximation[42] of the scattering profile yields the radius of gyration (R_g) of the particle in solution and indicates its elongation or compactness. Fourier transformation of the scattering profile gives the distance distribution function p(r) as a function of scattering distance r. This is characterised by one or maxima (M) and the maximum dimension of the scattering particle (D_{max}) both of which are characteristic features of the particle in solution: the algorithm in GNOM[41] allows to calculate p(r) as well as a further estimate for R_g (encouragingly R_g values from this procedure which were consistent with those from the Guinier analysis).

Using these procedures a radius of gyration of 26.4 Å was found for the murine γ1 Fab', similar to the previous determination.[61] Comparing the PEGylated conjugates with their parent antibodies (Table 2), scattering data have shown that the effect of PEGylation is to contribute to a more "extended" conformation in solution as indicated by the higher R_g and D_{max} values. By attaching two linear 20 kDa PEG to the C-termini of the heavy and light chains of the murine γ1 Fab', the resulting conjugate *mFab'-(L)PEG2 × 20k* has a D_{max} of 94 Å, suggesting a ~20 Å increase compared to the murine γ1 Fab'. The radius of gyration data are consistent with the D_{max} implying that the PEGylated molecule is more elongated. More pronounced differences were found between the human γ1 F(ab')$_2$ and *DFM-(Br)PEG2 × 20k*, with a ~9 Å increase in R_g and a ~30 Å increase in D_{max}.

The distance distribution function p(r) of a scattering particle reflects the shape and mass distribution of the molecule.[29,62] Figures 10 and 11 show the superimpositions of the p(r) function of the antibody fragments and their PEGylated conjugates. The p(r) function represents the distribution of all intra-particle scattering vectors and therefore the maximum M in p(r) corresponds to the most frequently occurring interatomic distance within the molecular structure.[29,63] Murine γ1 Fab' and *mFab'-(L)PEG2 × 20k* both have this maximum M at a value of r of ~30 Å (Fig. 10): this value refers to the most commonly occurring distance between the scattering centres in a single Fab'. Thus we can conclude that no significant conformational change to the antibody fragment occurs upon PEGylation, that is, the structure of the Fab' fragment itself remains essentially unaltered. Parts of the PEGylated molecule extend

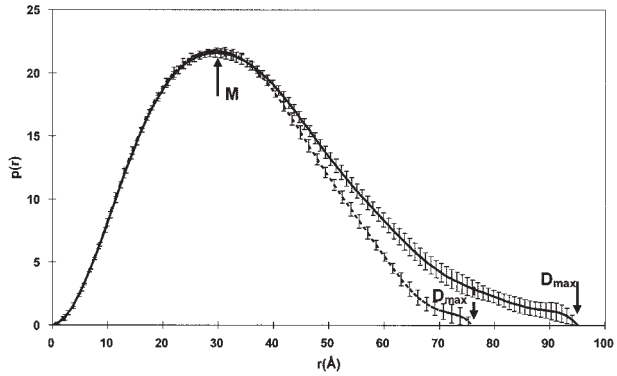

Figure 10. Superimposition of the experimental p(r) functions (with error bars) of murine γ1 Fab' (- - -) and *mFab-(L)PEG2 × 20k* (—). Both molecules have the same peak M at ~30Å. The maximum dimensions D_{max} are 76 and 95 Å respectively.

over larger distances (e.g. between the PEG moiety and the protein) and therefore contribute to the distribution of longer distances in the p(r) function which result in an increase in R_g and D_{max} compared to the isolated Fab' fragment.

Similarly, there is little tendency for the Fab' domain within *DFM-(Br)PEG2 × 20k* to undergo considerable conformation changes when compared to the human γ1 F(ab')$_2$. Analogous positions of the first maxima $M1$ are found at (32–35) Å (Fig. 11) that can be assigned to the most commonly occurring distance within a single Fab'. The second maximum peak $M2$ describes the most common distance within the whole molecule and therefore can be ascribed to the distance between

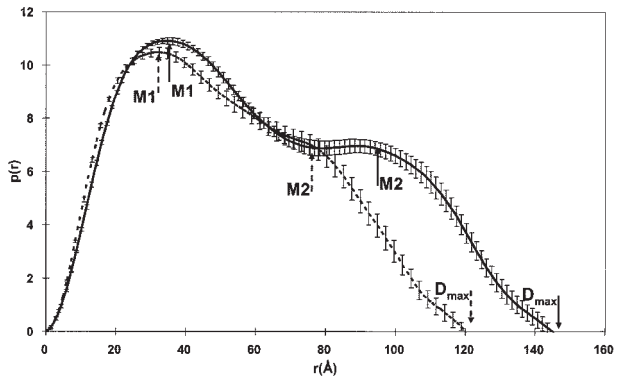

Figure 11. Superimposition of the experimental p(r) functions (with error bars) of human γ1 F(ab')$_2$ (- - -) and *DFM-(Br)PEG2 × 20k* (—). For human γ1 F(ab')$_2$, peaks M1 and M2 occur at ~32 Å and ~75 Å respectively, with D_{max} ~120 Å. For *DFM-(Br)PEG2 × 20k* peaks M1 and M2 occur at r_{M1} ~35 Å and r_{M2}~90 Å respectively, with D_{max} ~145 Å.

the two Fab's. As a bis-maleimide linker was used for the synthesis of *DFM-(Br)PEG2 × 20k*, an increase of 15 Å in peak *M*2 of *DFM-(Br)PEG2 × 20k* (90 Å) compared to the human γ1 $F(ab')_2$ (75 Å) illustrates the conformational variation between these two molecules due to the adduct of the bis-maleimide derivative of the branched PEG.

DISCUSSION

Ab Initio Modelling

Ab initio shape reconstruction using the program DAMMIN[43] was carried out to visualise the conformations of the antibodies and their PEGylated conjugates in solution For each molecule, 10 low resolution models obtained from different DAMMIN runs were analysed and the stable constructions (NSD < 0.8) were averaged that yielded a model representing the most probable features of the solution (see Materials and Methods Section).

To examine the validity of the shape reconstruction, the *ab initio* model of the murine γ1 Fab' was compared with the crystallographic models of two Fab' molecules (accession code 1UCB and 1BBJ respectively). Superimpositions of the *ab initio* model of murine γ1 Fab' with the crystallographic models using SUPCOMB[47] and MASSHA[48] are in very good agreement with all three Fab' models and have a similar volume (an example see Fig. 12). The scattering properties of the crystallographic models of two Fab' molecules (accession code 1UCB and 1BBJ respectively) were calculated using CRYSOL[45] and HYDROPRO[46] (data not shown). Superimposition of the p(*r*) functions (see Fig. 13) for the three different Fab' models yield similar positions for the maxima M and D_{max} and reflect the excellent harmony revealed between *ab initio* models and crystal structures (Fig. 12).

Correspondingly, *ab initio* models of *mFab-(L)PEG2 × 20k* and *hFab'-(L)PEG25k* were calculated and superimposed with the model of the murine γ1 Fab' (see Figs. 14 and 15). Distinct structural features are revealed in the

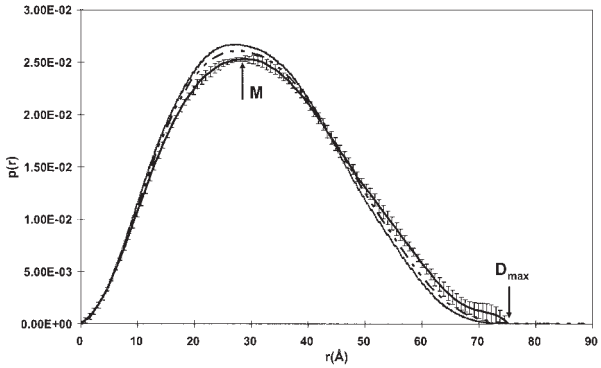

Figure 13. Superimposition of experimental p(*r*) function (with error bars) of the murine γ1 Fab' with p(r) functions of two Fab' crystallographic models calculated from HYDROPRO[46]: 1UCB (—··—··) and 1BBJ (·· ·· ··). For the murine γ1 Fab', the maximum M occurs at ~30 Å and the maximum dimensions D_{max} occurs at ~76 Å respectively.

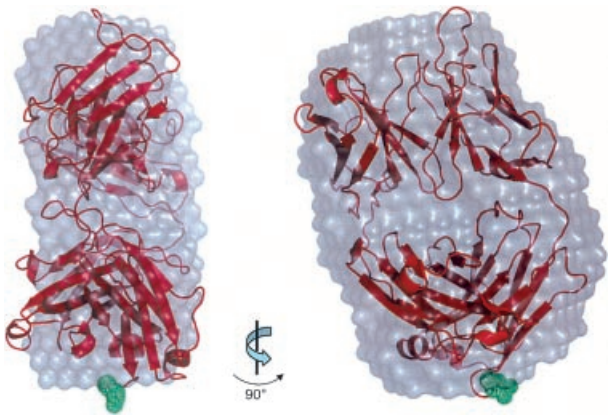

Figure 12. Superimposition of the Fab' crystal structure (PDB accession code 1UCB, red cartoon) with the *ab initio* model of murine γ1 Fab' (grey spheres). The cysteine in the light chain at position 214 is highlighted by green spheres.

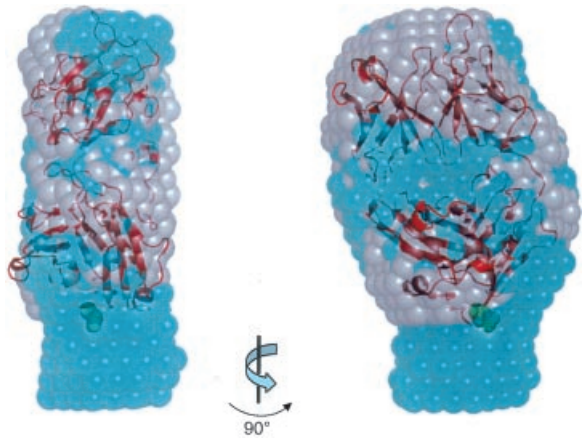

Figure 14. Superimposition of *ab initio* models of mFab-(L)PEG2 × 20k (transparent cyan spheres) with murine γ1 Fab' (transparent grey spheres). For orientation the red ribbon model represents the Fab' crystal structure as shown in Figure 9.

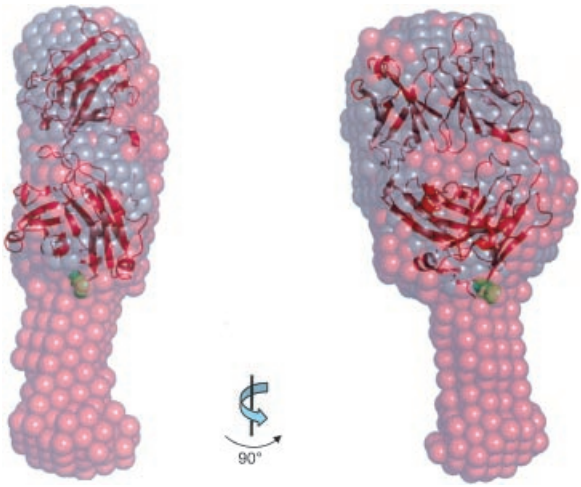

Figure 15. Superimposition of *ab initio* models of hFab'-(L)PEG25 k (transparent pink spheres) with murine γ1 Fab' (transparent grey spheres). For orientation the red ribbon model represents the Fab' crystal structure in analogy to Figures 9 and 11. Figures 9,11 and 12 were produced with the routine *PYMOL*.[65]

superimpositions of the Fab' with PEGylation conjugates and clearly demonstrates that the Fab' is essentially unchanged by PEGylation. The extension in the PEGylated model is attributed to the conjugation of PEG. However, it is apparent that the increase in volume of the PEGylated model is smaller than expected considering the size of the PEG moiety. With the significant increase in frictional ratio as observed by sedimentation velocity, it might be anticipated that the PEGylated molecule being much more "extended" or occupying a larger excluded volume. An explanation can be found in the fact that the PEG molecules are highly dynamic and flexible in solution and primarily the immediate interaction regions with the antibody will contribute to a strong scattering contrast between solvent and macromolecule. Besides, the shape restoration procedure with DAMMIN works more reliably for compact and rigid molecular configurations and it may be less sensitive to loosely bound and dynamically disordered structural arrangements.[64] Moreover, as the electron density within a PEGylated molecule is not homogeneous and is characterised by high solvation, the scattering contrast between the PEG moiety and the solvent is smaller compared to the one between protein and solvent.

This deviation from the expected particle volume suggests that the *ab initio* restoration does not represent fully the effective volume of the whole PEGylated molecule. Considering the above reasons it could be inferred that only the more ordered and rigid parts of the PEG moieties have been manifested in the shape calculations: contributions on the other hand from the dynamically disordered PEG segments had a contrast for X-rays that were only marginally higher than that for the buffer solution. Further studies involving contrast variation small angle neutron scattering (SANS) may help to resolve the issue on the conformation and contribution of the PEG moiety. Although SAXS fails to reveal details about the conformation of the whole PEG component, nonetheless it is still possible to comment on the way PEG is bound to the protein. For instance, models of *mFab'-(L)PEG2 × 20k* and *hFab'-(L)PEG25k* have shown that the attached PEG moiety extends from one end of the Fab'. A superimposition of the crystallographic models with the *ab initio* model of *hFab'-(L)PEG25k* is achievable so that the PEG moiety is attached to the Fab' fragment through the free cysteine that is exposed at the C-termini of the Fab' molecule (see Fig. 9). This is consistent with the conjugation chemistry applied in site-specific PEGylation (Fig. 2).

Concluding Remarks

AUC and measurement of the translational frictional ratio has shown that for all PEGylated-antibody fragment complexes studied, the hydrodynamic properties are dominated by the PEG moiety. SAXS at low values of r (distance between scattering centres) as manifested by the r_M and R_g values, indicate that the conformation of Fab' itself is essentially unchanged by incorporation into the complex. The globular Fab' therefore appears to "sit" inside the flexible PEG: although attached at a specific point, because of its much greater flexibility the time-averaged flexible conformation of the PEG may effectively cover part or all of the Fab'.

ACKNOWLEDGMENTS

We thank the United Kingdom Engineering and Physical Science Research Council for supporting this work, and the Council for the Central Laboratory of the Research Councils for access to the SRS, Daresbury. We thank Alistair Henry at UCB-Celltech (Slough, UK) for useful discussions, Helen

Brand and Gayle Phillips, also at UCB-Celltech (Slough, UK) for help in the purification and PEGylation of the Fab' fragments and Dr. Gordon Morris (NCMH) for the SEC-MALLs check on our molecular weights.

REFERENCES

1. Holliger P, Hudson PJ. 2005. Engineered antibody fragments and the rise of single domains. Nat Biotechnol 23:1126–1136.
2. King DJ, Adair JR, Angal S, Low DC, Proudfoot KA, Lloyd JC, Bodmer M, Yarranton GT. 1992. Expression, purifucation and characterisation of a mouse:human chimeric antibody and chimeric Fab' fragment. Biochem J 281:317–323.
3. Sun CZ, Wirsching P, Janda KD. 2003. Enabling ScFv as multi-drug carriers: A dendritic approach. Bioorg Med Chem 11:1761–1768.
4. Skerra A, Pluckthun A. 1988. Assembly of a functional immunoglobulin Fv fragment in Escherichia coli. Science 240:1038–1041.
5. Carter P, Kelley RF, Rodrigues ML, Snedecor B, Covarrubias M, Velligan MD, Wong WLT, Rowland AM, Kotts CE, Carver ME, Yang M, Bourell JH, Shepard HM, Henner D. 1992. High level Escherichia coli expression and production of a bivalent humanized antibody fragment. Bio/Technology 10:163–167.
6. King DJ, Turner A, Farnsworth AP, Adair JR, Owens RJ, Pedley RB, Baldock D, Proudfoot KA, Lawson AD, Beeley NR. 1994. Improved tumor targeting with chemically cross-linked recombinant antibody fragments. Cancer Res 54:6176–6185.
7. Casey JL, King DJ, Chaplin LC, Haines AM, Pedley RB, Mountain A, Yarranton GT, Begent RH. 1996. Preparation, characterisation and tumour targeting of cross-linked divalent and trivalent antitumour Fab' fragments. Br J Cancer 74:1397–1405.
8. Chen J, Jaracz S, Zhao X, Chen S, Ojima I. 2005. Antibody-cytotoxic agent conjugates for cancer therapy. Expert Opin Drug Deliv 2:873–890.
9. Chapman AP, Antoniw P, Spitali M, West S, Stephens S, King DJ. 1999. Therapeutic antibody fragments with prolonged in vivo half-lifes. Nat Biotechnol 17:780–783.
10. Chapman AP. 2002. PEGylated antibodies and antibody fragments for improved therapy: A review. Adv Drug Deliver Rev 54:531–545.
11. Koumenis IL, Shahrokh Z, Leong S, Hsei V, Deforge L, Zapata G. 2000. Modulating pharmacokinetics of an anti-interleukin-8 $F(ab')_2$ by amine-specific PEGylation with preserved bioactivity. Int J Pharm 198:83–95.
12. Tsutsumi Y, Onda M, Nagata S, Lee B, Kreitman RJ, Pastan I. 2000. Site-specific chemical modification with polyethylene glycol of recombinant immunotoxin anti-Tac(Fv)-PE38 (LMB-2) improves antitumor activity and reduces animal toxicity and immunogenicity. PNAS 97:8548–8553.
13. Delgado C, Pedley RB, Herraez A, Boden R, Boden JA, Keep PA, Chester KA, Fisher D, Begent RHJ, Francis GE. 1996. Enhanced tumour specificity of an anti-carcinoembrionic antigen Fab' fragment by poly(ethylene glycol) (PEG) modification. Br J Cancer 73:175–182.
14. Bailon P, Berthold W. 1998. Polyethylene glycol—conjugated pharmaceutical proteins. Pharmaceut Sci Technol Today 1:352–356.
15. Harris JM, Chess RB. 2003. Effect of PEGylation on pharmaceuticals. Nat Rev Drug Discov 2:214–221.
16. Harris JM. 1992. Introduction to biotechnical and biomedical applications of poly(ethylent glycol). In: Harris JM, editor. Poly(ethylene glycol) chemistry: Biotechnical and biomedical applications. Plenum Press. New York: pp 1–29.
17. Zalipsky S, Harris JM. 1997. Introduction to chemistry and biological applications of poly(ethylene glycol). In: Harris JM, Zalipsky S, editors. Poly(ethylene glycol) chemistry and biological applications. Washington, DC: American Chemical Society. pp 1–5.
18. Roberts MJ, Bentley MD, Harris JM. 2002. Chemistry for peptide and protein PEGylation. Adv Drug Deliver Rev 54:459–476.
19. Wang Y, Youngster S, Grace M, Bausch J, Bordens R, Wyss DF. 2002. Structural and biological characterization of pegylated recombinant interferon alpha-2b and its therapeutic implications. Adv Drug Deliver Rev 54:547–570.
20. Fee CJ, Van Alstine JM. 2006. PEG-proteins: Reaction engineering and separation issues. Chem Eng Sci 61:924–939.
21. Fee CJ, Van Alstine JM. 2004. Prediction of the viscosity radius and the size exclusion chromatography behavior of PEGylated proteins. Bioconjugate Chem 15:1304–1313.
22. Kodera Y, Matsushima A, Hiroto M, Nishimura H, Ishii A, Ueno T, Inada Y. 1998. PEGylaion of protiens and bioactive substances for medical and technical applications. Prog Polym Sci 23:1233–1271.
23. Rajender Reddy K, Modi MW, Pedder S. 2002. Use of peginterferon alfa-2a (40 KD) (Pegasys®) for the treatment of hepatitis C. Adv Drug Deliver Rev 54:571–586.
24. Charles SA, Harris JM, Pedder S, Kumar S. 2000. Improving hepatitis C therapy: Attaching a polyethylene glycol "tail" to interferon for better clinical properties. Mod Drug Discov 5:59–67.
25. Monfardini C, Schiavon O, Caliceti P, Morpurgo M, Harris JM, Veronese FM. 1995. A branced

monomethoxypoly(ethelene glycol) for protein modification. Bioconjugate Chem 6:62–69.
26. Veronese FM, Harris JM. 2002. Introduction and overview of peptide and protein pegylation. Adv Drug Deliver Rev 54:453–456.
27. In: Scott D, Harding SE, Rowe AJ, editors. 2005. Analytical ultracentrifugation: Techniques and methods. Cambridge: Royal Society of Chemistry.
28. In: Harding SE, Rowe AJ, Horton JC, editors. 1992. Analytical ultracentrifugation in biochemistry and polymer science. Cambridge: Royal Society of Chemistry. 629.
29. Glatter O, Kratky O. 1982. Small angle X-ray scattering. London: Academic Press.
30. Koch MHJ, Vachette P, Svergun DI. 2003. Small-angle scattering: A view on the properties, structures and structural changes of biological macromolecules in solution. Q Rev Biophys 36: 147–227.
31. Laue TM, Shah BD, Ridgeway TM, Pelletier SL. 1992. Computer-aided interpretation of analytical sedimentation data for proteins. In: Harding SE, Rowe AJ, Horton JC, editors. Analytical ultracentrifugation in biochemistry and polymer science. Royal Society of Chemistry. Cambridge: pp 90–125.
32. Lepori L, Mollica V. 1978. Volumetric properties of dilute aqueous solutions of poly(ethylene glycols). J Polym Sci 16:1123–1134.
33. Nichol LW, Ogston AG, Wills PR. 1981. Effect of inert polymers on protein self-association. FEBS Lett 126:18–20.
34. Durchschlag H, Zipper P. 2005. Calculation of volume, surface, and hydration properties of biopolymers. In: Scott D, Harding SE, Rowe AJ, editors. Analytical ultracentrifugation: Techniques and methods. Royal Society of Chemistry. Cambridge: pp 389–431.
35. Schuck P. 2000. Size distribution analysis of macromolecules by sedimentation velocity ultracentrifugation and Lamm equation modeling. Biophys J 78:1606–1619.
36. Dam J, Schuck P. 2004. Calculating sedimentation coefficient distributions by direct modeling of sedimentation velocity concentration profiles. Methods Enzymol 384:185–212.
37. Rowe AJ. 1992. The concentration dependence of sedimentation. In: Harding SE, Rowe AJ, Horton JC, editors. Analytical ultracentrifugation in biochemistry and polymer science. Royal Society of Chemistry. Cambridge: pp 394–406.
38. Cölfen H, Harding SE. 1997. MSTARA and MSTARI: Interactive PC algorithms for simple, model independent evaluation of sedimentation equilibrium data. Eur Biophys J 25:333–346.
39. Creeth JM, Harding SE. 1982. Some observations on a new type of point average molecular weight. J Biochem Biophys Methods 7:25–34.
40. Boulin CJ, Kempf R, Gabriel A, Koch MHJ. 1988. Data acquisition systems for linear and area x-ray detectors using delay-line readout. Nucl Instr Meth Phys Res 269:312–320.
41. Semenyuk AV, Svergun DI. 1991. GNOM-a program package for small-angle scattering data processing. J Appl Crystal 24:537–540.
42. Guinier A, Fournet G. 1995. Small angle scattering of X-rays. Wiley: New York.
43. Svergun DI. 1999. Restoring low resolution structure of biological macromolecules from solution scattering using simulated annealing. Biophys J 76:2879–2886.
44. Volkov VV, Svergun DI. 2003. Uniqueness of ab initio shape determination in small-angle scattering. J Appl Cryst 36:860–864.
45. Svergun DI, Barberato C, Koch MHJ. 1995. CRYSOL-a program to evaluate x-ray solution scattering of biological macromolecules from atomic coordinates. J Appl Cryst 28:768–773.
46. Garcia de la Torre J, Huertas ML, Carrasco B. 2000. Calculation of hydrodynamic properties of globular proteins from their atomic-level structure. Biophys J 78:719–730.
47. Kozin MB, Svergun DI. 2000. Automated matching of high- and low-resolution structural models. J Appl Cryst 34:33–41.
48. Konarev PV, Petoukhov MV, Svergun DI. 2001. MASSHA-a graphics system for rigid-body modelling of macromolecular complexes against solution scattering data. J Appl Cryst 34:527–532.
49. Heymann B, Grubmuller H. 1999. Elastic properties of poly(ethylene-glycol) studied by molecular dynamics stretching simulations. Chem Phys Lett 307:425–432.
50. Chew B, Couper A. 1976. Diffusion, Viscosity and sedimentation of poly(ethylene oxide) in water. J Chem Soc, Faraday Trans 72:382.
51. Branca C, Magazu S, Maisano G, Migliardo P, Migliardo F, Romeo G. 2002. Hydration parameters of aqueous solutions of poly(ethylene glycol)s by viscosity data. Physica Scripta 66:175– 179.
52. Bailey FE, Callard RW. 1959. Some properties of poly(ethylene oxide) in aqueous solution. J Appl Polym Sci 1:56–62.
53. Branca C, Magazu S, Maisano G, Migliardo F, Migliardo P, Romeo G. 2003. Study of conformational properties of poly(ehtylene oxide) by SANS and PCS techniques. Physica Scripta 67:551–551.
54. Maron SH, Filisko FE. 1972. Heats of solution and dilution for poly(ethylene oxide) in several solvents. J Macromol Sci Phys 6:79–90.
55. Smidrsød O, Andresen IL. 1979. Biopolymerkjemi. Trondheim, Norway: Tapir Press.
56. Fujita H. 1962. Mathematical theory of sedimentation analysis. Academic Press. New York: 315.

57. van Holde KE. 1985. Chapter 5: Sedimentation. Physical Biochemistry. Prentice-Hall, Inc. New Jersey: pp 110–133.
58. Harding SE, Cölfen H, Aziz Z. 2005. The ELLIPS suite of whole-body protein conformation algorithms for Microsoft Windows. In: Scott D, Harding SE, Rowe AJ, editors. Analytical ultracentrifugation techniques and methods. Royal Society of Chemistry. Cambridge: pp 468–483.
59. Carrasco B, Garciade la Torre J, Byron O, King D, Walters C, Jones S, Harding SE. 1999. Novel size-independent modeling of the dilute solution conformation of the immunoglobulin IgG Fab' domain using SOLPRO and ELLIPS. Biophys J 77:2902–2910.
60. Lu Y. 2007. PhD Thesis: Solution conformation of engineered antibodies. School of Biosciences, ed., Nottingham: University of Nottingham
61. Morgan PJ, Byron OD, Harding SE. 1992. The solution conformation of novel antibody fragments studied using analytical ultracentrifugation. Discovery 1–4. (Beckman Instruments, Palo Alto, USA) DS-834.
62. Svergun DI. 1992. Determination of the regularisation parameter in indirect transform using perceptual criteria. J Appl Crystal 25:495–503.
63. Furtado PB, Whitty PW, Robertson A, Eaton JT, Almogren A, Kerr MA, Woof JM, Perkins SJ. 2004. Solution structure determination of monomeric human IgA2 by X-ray and neutron scattering, analytical ultracentrifugation and constrained modelling: A comparison with monomeric human Ig A1. J Mol Biol 338:921–941.
64. Zipper P, Durchschlag H, Krebs A. 2005. Modelling of Biopolymers. In: Scott D, Harding SE, Rowe AJ, editors. Analytical ultracentrifugation: Techniques and methods. Royal Society of Chemistry. Cambridge: pp 320–371.
65. DeLano WL. 2002. The PyMOL Molecular Graphics System. DeLano Scientific. San Carlos. CA, USA, http://wwwpymolorg.